NASA Technical Memorandum 78587

(NASA-TM-78587) INTERFERENCE EFFECTS OF AIRCRAFT COMPONENTS ON THE LOCAL BLADE ANGLE OF ATTACK OF A WING-MOUNTED PROPELLER (NASA) 43 p HC A03/MF A01 CSCL 01C

N79-25021

Unclas

G3/07 23466

Interference Effects of Aircraft Components on the Local Blade Angle of Attack of a Wing-Mounted Propeller

J. P. Mendoza

June 1979

National Aeronautics and
Space Administration

NASA Technical Memorandum 78587

Interference Effects of Aircraft Components on the Local Blade Angle of Attack of a Wing-Mounted Propeller

J. P. Mendoza, Ames Research Center, Moffett Field, California

NASA
National Aeronautics and
Space Administration

Ames Research Center
Moffett Field, California 94035

NOMENCLATURE

A	matrix for rotation about the y-axis
B	matrix for rotation about the z-axis
b	wing span, m
c	chord, m
$\bar{c}$	mean aerodynamic chord, m
i_α	propeller or nacelle incidence (body centerline reference), deg
i_β	propeller or nacelle yaw angle, deg (see fig. 1(b))
M	Mach number
N	nacelle with simulated jet exhaust
P	propeller
R	radius of propeller disc, m
r	radial distance along propeller blade, m
t	airfoil thickness, m
U	column vector (see appendix A)
u	velocity in the x-direction, m/sec
u_1,u_2,u_3	components of the U-column vector
V	transformed column vector, V = AU
V_∞	free-stream velocity, m/sec
v	velocity in the y-direction, m/sec
v_N	(see fig. 4)
v_1,v_2,v_3	components of the V-column vector
W	transformed column vector, W = BV
W_1	rectangular wing
W_2	swept wing
W_3	tapered wing with a crank trailing edge

W_4	twisted and cambered wing
w	velocity in the z-direction, m/sec
w_1, w_2, w_3	components of the W-column vector
x, y, z	Cartesian coordinates
α	angle of attack, deg
α_L	propeller blade angle of attack at $\frac{r}{R} = 0.75$, deg
β	propeller blade pitch angle at $\frac{r}{R} = 0.75$, deg
$\Delta_{\alpha L}$	difference between maximum and minimum values of α_L
ψ	azimuth angle, deg (see fig. 3)
ϕ	(see fig. 4)
ω	rotational velocity, rad/sec
ζ, η, ξ	(see fig. 3)

INTERFERENCE EFFECTS OF AIRCRAFT COMPONENTS ON THE LOCAL BLADE ANGLE OF ATTACK OF A WING-MOUNTED PROPELLER

J. P. Mendoza

Ames Research Center

SUMMARY

A brief theoretical study was conducted at $M = 0.6$ to obtain an understanding of the aerodynamic interference effects on a propeller operating in the presence of different wing-body-nacelle combinations. The study was directed toward minimizing the unsteady blade angle-of-attack variation with azimuth angle by varying the pitch and yaw of the nacelle. For the particular configuration of interest the minimum blade angle-of-attack variation occurred with the nacelle pitched downward 4.5° and yawed inward 3.0°.

INTRODUCTION

Since 1973, the fuel fraction of the direct operating cost for air transports has been steadily increasing, thus creating the need for fuel-efficient airplanes (ref. 1). Studies have indicated that a turboprop-powered airplane operating at $M = 0.8$ could achieve a 10-20% savings in fuel relative to a comparable turbofan-powered airplane. For this reason, research efforts are currently underway in categories such as advance propellers, propeller noise and fuselage noise attenuation, propeller and gearbox maintenance, and airframe-propulsion systems integration. In this last category, both theoretical (ref. 2) and experimental (ref. 3) investigations have been conducted to determine the propeller slipstream effects on wing-body-nacelle- and wing-body combinations, respectively. One aspect of airframe-propulsion systems integration that has not been widely investigated is the problem of the interference effects on the propeller blade attributed to the presence of airplane components such as wings and bodies. In particular, the problem that has not been previously addressed is that of minimizing the cyclic bending moments applied to the propeller blade caused by the local blade angle-of-attack variation with azimuth angle. As a result, the present investigation was conducted: (1) to obtain a better understanding of the interference effects on the propeller blade due to the presence of wings and bodies and (2) to minimize the blade angle-of-attack variation with azimuth angle for a given turboprop transport model.

AIRPLANE COMPONENTS

The five different configurations used in the present theoretical study are shown in figures 1 and 2. They include an isolated nacelle with a simulated jet exhaust (fig. 1) and four different wing-body-nacelle configurations, also with simulated jet exhausts (figs. 2(a) through 2(c)). As noted in figure 2(c), two of the configurations (PBW_3N and PBW_4N) were identical except for wing camber and twist. The wing sections for the configurations with the rectangular and swept wings had the same thickness distribution. The airfoil coordinates are presented in table 1. The coordinates for the tapered wing with the crank trailing edge are shown in table 2 for four span stations. The coordinates at four span stations for the cambered and twisted wing which had the same planform as the tapered wing are presented in table 3. Each of the four wings had 2° of dihedral. The nacelle was pitched and yawed about the fixed reference point shown in figure 1.

METHOD

Because a generalized method is not presently available, an approximate method was developed for estimating the interference effects of nearby airplane components on the local angle of attack of a propeller blade. The method is based on the assumption that the inflow into the propeller disc is dominated by the aircraft configuration and is essentially independent of the propeller and its slipstream. Under this assumption, the local inflow velocities can be combined vectorially with the rotational velocity of the propeller blade to define a local blade angle of attack as a function of azimuth angle. The method used to predict the local flow velocities was the Douglas-Neumann Potential Flow Program (ref. 4) which is a linear panel method capable of analyzing complete aircraft configurations. Using this method, velocities are computed at off-body points corresponding to points at $r/R = 0.75$ on the propeller blade at different azimuth angles. The point at $r/R = 0.75$ coincides with the centroid of the load distribution of the propeller blade and the flow at this point is considered to be representative of that for the entire blade.

The problem of minimizing the cylic bending moments of the propeller blade caused by the variation in the local angle of attack of the blade is a difficult problem in itself. The difficulty is increased at higher subsonic Mach numbers where transonic effects are present and no adequate transonic analysis is presently available. To simplify the problem and allow the use of linear methods, it was assummed that the local angle-of-attack variation of the propeller blade at $M = 0.8$ is essentially the same as that at $M = 0.6$ for the same velocity ratio which is the ratio of the tip velocity to the free-stream velocity. The velocity ratio was 1.0. The design blade pitch angle, $\beta_{0.75R}$, of 56.5° at $M = 0.6$ was used throughout the present study.

Shown in figures 3(a) and 3(b) are the flow velocities at a point on the propeller blade. The propeller, unless otherwise noted, has right-hand rotation (counterclockwise as seen by an observer in front of the airplane) and is installed on the right wing panel. The flow velocities which are computed by the method of reference 4 are transformed by the procedure described in appendix A into the w_1, w_2, and w_3 components shown in figure 3(a). These components, in turn, are resolved into velocity components along the axes of a coordinate system that rotates with the propeller. Two of the three components are shown in figure 3(b). The third component that is parallel to the radius of the propeller does not contribute to the blade bending moment and, therefore, is not included in the analysis. From figure 3(b)

$$v_N = r\omega - w_2 \sin \psi - w_3 \cos \psi$$

Since

$$\phi = \tan^{-1}(w_1/v_N)$$

then α_L, the local angle of attack of the blade is given by

$$\alpha_L = \beta - \phi$$

where β is the propeller pitch angle.

RESULTS

Component Buildup

To obtain a better understanding of the interference effects on the propeller blade attributed to the presence of nearby airplane components such as wings and bodies, an airplane component buildup was conducted starting with an isolated propeller and continuing on to wing-body-nacelle configurations with varying wing geometry. Blade angle-of-attack variations with azimuth angle were compared for the different configurations. By using the results of the isolated propeller study as a basis for comparison, the effects of adding or changing various airplane components can be assessed. The local angle of attack of the propeller blade is understood to be computed at $r/R = 0.75$.

Figure 4 shows the variation of the local angle of attack of the propeller blade with azimuth angle for an isolated propeller in a uniform flow field. The solid line represents the condition where the propeller axis of rotation is aligned with the free-stream velocity vector, while the dashed line represents the condition where the propeller axis of rotation is pitched upward 2° which is observed to produce a $\Delta\alpha_L$ of 2.5°.

Figure 5 shows the results for an isolated propeller P and for a propeller in the presence of a nacelle with a simulated jet exhaust PN. In both cases the propeller axis is at $i_\alpha = 0°$. The asymmetry of the nacelle induces nearly 1° of unsteady blade angle-of-attack variation. Figure 6 shows the effects of pitch angle on the PN configuration. Note the variation in $\Delta\alpha_L$ with varying i_α. The smallest value of $\Delta\alpha_L$ is at $i\alpha = -0.5°$.

Comparison of the blade angle-of-attack characteristics for the configuration buildup is shown in figure 7 starting with an isolated nacelle and continuing on to a rectangular wing-body-nacelle configuration, PBW_1N. For this comparison the body and wing are at 2° angle of attack and the nacelle is pitched downward 2.5° relative to the body centerline (-0.5° relative to the free stream). Note the small contribution of the body to the overall level of α_L which is in sharp contrast to the effect due to the wing with its attendant upwash field.

Figure 8 shows the effects of varying nacelle pitch angle on the blade angle-of-attack characteristics for the rectangular wing-body-nacelle configuration, PBW_1N. The wing and body are at 2° angle of attack while the nacelle is pitched from -2.5° to -4.0°. The smallest value of $\Delta\alpha_L$ occurs at $i_\alpha = -3.5°$.

Figure 9 shows the effect of wing sweep. Blade angle-of-attack characteristics for wing-body-nacelle configurations with a rectangular wing (PBW_1N) and a swept wing (PBW_2N) are compared. The wings and bodies are at 2° angle of attack and the nacelles are at $i_\alpha = -3.5°$. The sweep angle for the swept wing was 35°. Wing sweep is shown to produce a substantial increase in $\Delta\alpha_L$ because of the sidewash that is induced by a wing sweep. To compensate for the effects of sidewash induced by wing sweep, the nacelle for the swept-wing configuration (PBW_2N) was yawed from 0° to 2.5°. The results are shown in figure 10. The wing and body are at 2° angle of attack and the nacelle is at $i_\alpha = -3.5°$. The smallest value of $\Delta\alpha_L$ is at $i_\beta = 2°$.

The effects of wing planform on the blade angle-of-attack characteristics were investigated using the swept wing-body-nacelle configurations PBW_2N and PBW_3N. The results that are shown in figure 11 show a small change in the blade angle-of-attack characteristics as a result of the change in wing planform. A comparison of the blade angle-of-attack characteristics for the tapered wing-body-nacelle configuration with and without camber and twist is shown in figure 12. The significant changes shown in the blade angle-of-attack characteristics for the cambered and twisted wing are produced by the change in the induced upwash field of the wing.

Blade Angle-of-Attack Minimization

In the present investigation, the procedure used to minimize the cyclic bending moments applied to the propeller blades of a turboprop transport model is to minimize $\Delta\alpha_L$. Except for the addition of nacelles and simulated jet exhausts, the PBW_4N configuration is the same as that used in the investigation reported in reference 3. Since it has been shown that $\Delta\alpha_L$ can be minimized by varying the pitch and/or yaw of the nacelle, the nacelle of the PBW_4N configuration was yawed from 2° to 3.5° in 0.5° increments. At each yaw angle the nacelle was pitched from -2.5° to -5.5° in 1° increments. The results of this study are shown in figures 13(a) through 13(d) and the data for these figures are summarized in figure 14. This shows values of $\Delta\alpha_L$ for each combination of pitch and yaw angles. The minimum value was found to be 2° and corresponds to $i_\alpha = -4.5°$ and $i_\beta = 3.0°$.

To determine the effect of reverse propeller rotation which corresponds to a propeller with right-hand rotation mounted on the left wing panel, blade angle-of-attack characteristics for the PBW_4N configuration are compared for the propellers with counterclockwise and clockwise (reverse) rotations. The body and wing are at $\alpha = 2°$ and the nacelle is at $i_\alpha = -4.5°$ and $i_\beta = 3.0°$ which are the optimum pitch and yaw angles for minimum $\Delta\alpha_L$ for the counterclockwise rotating propeller. Figure 15 shows that in addition to the expected change in phase angle there is an increase in $\Delta\alpha_L$ from 2° to 3° (reverse rotation).

CONCLUSIONS

The interference effects on the propeller attributed to the presence of different airplane components such as wings and bodies (including nacelles with simulated jet exhausts) were found to affect the blade angle-of-attack characteristics significantly. Compared to the effect of varying the inclination of the propeller axis of rotation, however, these effects are not as large. Each component is shown to affect the blade angle of attack to some extent. The largest component effect came from the wing. The minimum value of $\Delta\alpha_L$ for the PBW_4N configuration was obtained with a nacelle orientation of $i_\alpha = -4.5°$ and $i_\beta = 3.0°$.

APPENDIX A

As previously described, the nacelle can be pitched and yawed about a fixed reference point (fig. 1). For given values of i_α and i_β, velocities can be computed (using the method of reference 4) at off-body points corresponding to points on the propeller blade. To compute the local blade angle of attack, these velocities are resolved into components along the axes of a rotating orthogonal system of coordinates (ζ,η,ξ) shown in the inset in figure 3. Let (x,y,z) be the coordinates of a point on the propeller blade at $r/R = 0.75$ for a given azimuth angle. The column vector U represents the velocity components. Matrix A is the i_α rotation matrix and V represents the transformed vector. The transformation is given by

$$V = AU \tag{1}$$

If B represents the i_β rotation matrix, the final transformed vector is W. This transformation is given by

$$W = BV \tag{2}$$

The final transformed vector W is related to U by

$$W = BAU \tag{3}$$

Equation (1) may be written as

$$\begin{bmatrix} v_1 \\ v_2 \\ v_3 \end{bmatrix} = \begin{bmatrix} \cos i_\alpha & 0 & \sin i_\alpha \\ 0 & 1 & 0 \\ -\sin i_\alpha & 0 & \cos i_\alpha \end{bmatrix} \begin{bmatrix} u_1 \\ u_2 \\ u_3 \end{bmatrix}$$

The u_1, u_2, and u_3 are the x, y, and z velocity components given by the method of reference 4 at the point (x,y,z). Equation (2) may be written as

$$\begin{bmatrix} w_1 \\ w_2 \\ w_3 \end{bmatrix} = \begin{bmatrix} \cos i_\beta & \sin i_\beta & 0 \\ -\sin i_\beta & \cos i_\beta & 0 \\ 0 & 0 & 1 \end{bmatrix} \begin{bmatrix} v_1 \\ v_2 \\ v_3 \end{bmatrix}$$

Here the w_1, w_2, and w_3 are the velocity components that are shown in figure 3.

APPENDIX B

To verify the results of the present investigation, velocities at off-body points that were computed by the method of reference 4 were compared to those computed by two different methods, one of which was the transonic potential flow solution of Jameson (ref. 6) and the other was the modified small disturbance theory program (ref. 7). Since the Jameson method cannot treat wing-body configurations, a wing-alone case was computed using each of the three methods. The geometric characteristics of the wing alone is identical to the wing of the PBW_4N configuration from the 12% to the 100% semispan stations. The wing area of the wing-alone configuration is approximately equal to the exposed wing area of the PBW_4N configuration. The Jameson computer program was modified to print velocities at off-body mesh points in the sheared parabolic coordinate system. The mesh points were in a region in front of the wing, above and below the wing chord plane. The coordinates of the selected mesh points were used as inputs to the method of reference 4 which has the capability of computing velocities at arbitrarily specified off-body points, so that a direct comparison of the velocities can be made. Like the Jameson program the method of reference 7 does not have the capability of computing velocities at arbitrary off-body points. This computer program, however, was similarly modified to print velocities in a given region of the wing-alone flow field. Since the program has been designed to generate its own coordinate system, it was necessary to interpolate between mesh points to obtain velocities at given "Jameson mesh points." Shown in figures 16(a-c) are comparisons of the various velocity components. The $\Delta x/\bar{c}$ indicates the distance ahead of the wing leading edge. The coordinates have been normalized by the mean aerodynamic chord and the semispan of the PBW_4N configuration. All three methods agree fairly well with one another with the exception of the method of reference 7 which predicts lower values of the w/V_∞ than the other two methods.

Shown in figure 17 are the velocities at off-body points corresponding to points in the propeller disc at $r/R = 0.75$ for the wing-alone cases computed by the three different methods. Note that, as in the previous comparisons (fig. 16(c)), the overall level of the w/V_∞ component computed by the method of reference 7 is lower than the w/V_∞ levels computed by the methods of references 4 and 6. The effect of the differences in w/V_∞ on the blade angle-of-attack characteristics is shown in figure 18. The wing-alone velocities were adjusted for the effects of the body and nacelle using increments computed by the method of reference 4. The blade angle-of-attack characteristics based on the velocities computed by the methods of references 4 and 6 are shown to be in good agreement with each other while α_L based on the results of reference 7 shows a different overall level.

REFERENCES

1. Dugan, J. F.; Bencze, D. P.; and Williams, L. J.: Advanced Turboprop Technology Development. AIAA Aircraft Systems and Technology Meeting. Seattle, Washington. Aug. 22-24, 1977. AIAA Paper 77-1223.

2. Boctor, M. L.; Clay, C. W.; and Watson, C. F.: An Analysis of Prop-Fan/Airframe Aerodynamic Integration. NASA CR-152186, Oct. 1978.

3. Welge, H. R.; and Crowder, J. P.: Simulated Propeller Slipstream Effects on a Supercritical Wing. NASA CR-152138. June 1978.

4. Hess, J. L.: Calculation of Potential Flow About Arbitrary Three-Dimensional Lifting Bodies. Douglas Aircraft Co., Inc. Report MDC-J5679-01, Oct. 1972.

5. Mack, Dun-Pok: Calculation of Potential Flow About Arbitrary Three-Dimensional Lifting Bodies (User's manual) Douglas Aircraft Co., Inc. Report MDC-J5679-02. Oct. 1972.

6. Jameson, A.: Iterative Solution of Transonic Flows over Airfoils and Wings, Including Flow at Mach 1. Comm. Pure Appl. Math., vol. 27, no. 3, May 1974, pp. 283-309.

7. Mason, W. H.; Ballhaus, W. F.; Mackenzie, D.; Frick, J.; and Stern, M.: An Automated Procedure for Computing the Three Dimensional Transonic Flow over Wing-Body Combinations, Including Viscous Effects. AFFDL-TR-77, vols. I and II, Sept. 1977.

TABLE 1.— AIRFOIL COORDINATES FOR WINGS W_1 AND W_2

x/c	t/c	
	Upper surface	Lower surface
0.00000	0.00000	0.00000
.00961	.02406	-.02406
.02153	.03579	-.03579
.03806	.04677	-.04677
.05904	.05650	-.05650
.08427	.06450	-.06450
.11350	.07045	-.07045
.14645	.07432	-.07432
.18280	.07638	-.07638
.22222	.07695	-.07695
.26430	.07635	-.07635
.30866	.07476	-.07476
.35486	.07231	-.07231
.40246	.06908	-.06908
.45099	.06520	-.06520
.50000	.06074	-.06074
.54901	.05579	-.05579
.59755	.05047	-.05047
.64514	.04490	-.04490
.69134	.03918	-.03918
.73570	.03345	-.03345
.77770	.02782	-.02782
.81720	.02243	-.02243
.85355	.01744	-.01744
.88651	.01297	-.01297
.91574	.00912	-.00912
.94096	.00597	-.00597
.96194	.00353	-.00353
.99039	.00067	-.00067
1.00000	.00000	.00000

TABLE 2.— AIRFOIL COORDINATES FOR WING W_3

x/c	y/(b/2) = 0.12, t/c, Upper surface	y/(b/2) = 0.12, t/c, Lower surface	y/(b/2) = 0.35, t/c, Upper surface	y/(b/2) = 0.35, t/c, Lower surface	y/(b/2) = 0.70, t/c, Upper surface	y/(b/2) = 0.70, t/c, Lower surface	y/(b/2) = 1.00, t/c, Upper surface	y/(b/2) = 1.00, t/c, Lower surface
0.00000	0.00000	0.00000	0.00000	0.00000	0.00000	0.00000	0.00000	0.00000
.00961	.02406	−.02406	.01721	−.01721	.01675	−.01675	.01576	−.01576
.02153	.03579	−.03579	.02492	−.02492	.02425	−.02425	.02281	−.02281
.03806	.04677	−.04677	.03198	−.03198	.03112	−.03112	.02927	−.02927
.05904	.05650	−.05650	.03834	−.03834	.03730	−.03730	.03509	−.03509
.08427	.06450	−.06450	.04398	−.04398	.04279	−.04279	.04026	−.04026
.11350	.07045	−.07045	.04891	−.04891	.04759	−.04759	.04477	−.04477
.14645	.07432	−.07432	.05316	−.05316	.05173	−.05173	.04866	−.04866
.18280	.07638	−.07638	.05678	−.05678	.05526	−.05526	.05198	−.05198
.22222	.07695	−.07695	.05980	−.05980	.05819	−.05819	.05474	−.05474
.26430	.07635	−.07635	.06219	−.06219	.06052	−.06052	.05693	−.05693
.30866	.07476	−.07476	.06390	−.06390	.06218	−.06218	.05850	−.05850
.35486	.07231	−.07231	.06486	−.06486	.06311	−.06311	.05937	−.05937
.40246	.06908	−.06908	.06497	−.06497	.06322	−.06322	.05947	−.05947
.45099	.06520	−.06520	.06412	−.06412	.06239	−.06239	.05869	−.05869
.50000	.06074	−.06074	.06217	−.06217	.06050	−.06050	.05691	−.05691
.54901	.05579	−.05579	.05902	−.05902	.05743	−.05743	.05403	−.05403
.59755	.05047	−.05047	.05464	−.05464	.05316	−.05316	.05001	−.05001
.64514	.04490	−.04490	.04915	−.04915	.04783	−.04783	.04499	−.04499
.69134	.03918	−.03918	.04284	−.04284	.04169	−.04169	.03922	−.03922
.73570	.03345	−.03345	.03610	−.03610	.03513	−.03513	.03304	−.03304
.77779	.02782	−.02782	.02931	−.02931	.02852	−.02852	.02683	−.02683
.81720	.02243	−.02243	.02285	−.02285	.02224	−.02224	.02092	−.02092
.85355	.01744	−.01744	.01701	−.01701	.01656	−.01656	.01557	−.01557
.88651	.01297	−.01297	.01204	−.01204	.01172	−.01172	.01102	−.01102
.91574	.00912	−.00912	.00809	−.00809	.00787	−.00787	.00740	−.00740
.94096	.00597	−.00597	.00515	−.00515	.00501	−.00501	.00472	−.00472
.96194	.00353	−.00353	.00310	−.00310	.00302	−.00302	.00284	−.00284
.99039	.00067	−.00067	.00080	−.00080	.00078	−.00078	.00073	−.00073
1.00000	.00000	.00000	.00000	.00000	.00000	.00000	.00000	.00000

TABLE 3.— AIRFOIL COORDINATES FOR WING W_4

	y/(b/2) = 0.12		y/(b/2) = 0.35		y/(b/2) = 0.70		y/(b/2) = 1.00	
	t/c		t/c		t/c		t/c	
x/c	Upper surface	Lower surface	Upper surface	Lower surface	Upper surface	Lower surface	Upper surface	Lower surface
0.00000	0.00000	0.00000	0.00000	0.00000	0.00000	0.00000	0.00000	0.00000
.00961	.02362	−.02450	.01672	−.01771	.01625	−.01725	.01525	−.01626
.02153	.03485	−.03673	.02391	−.02594	.02323	−.02527	.02179	−.02383
.03806	.04496	−.04859	.03045	−.03351	.02958	−.03265	.02774	−.03081
.05904	.05354	−.05947	.03644	−.04024	.03540	−.03921	.03319	−.03700
.08427	.06063	−.06838	.04194	−.04601	.04076	−.04483	.03822	−.04230
.11350	.06600	−.07490	.04698	−.05083	.04567	−.04951	.04284	−.04670
.14645	.06952	−.07913	.05157	−.05476	.05014	−.05333	.04707	−.05026
.18280	.07135	−.08140	.05568	−.05788	.05416	−.05036	.05088	−.05308
.22222	.07190	−.08201	.05931	−.06029	.05770	−.05868	.05425	−.05523
.26430	.07161	−.08110	.06238	−.06201	.06070	−.06034	.05711	−.05675
.30866	.07075	−.07878	.06480	−.06301	.06308	−.06129	.05939	−.05760
.35486	.06939	−.07522	.06651	−.06321	.06476	−.06146	.06102	−.05772
.40246	.06750	−.07067	.06748	−.06246	.06573	−.06071	.06198	−.05696
.45099	.06504	−.06537	.06769	−.06054	.06597	−.05882	.06227	−.05512
.50000	.06197	−.05951	.06713	−.05721	.06546	−.05554	.06187	−.05195
.54901	.05830	−.05329	.06576	−.05228	.06417	−.05069	.06077	−.04728
.59755	.05406	−.04688	.06355	−.04572	.06208	−.04425	.05893	−.04110
.64514	.04932	−.04047	.06047	−.03782	.05915	−.03650	.05632	−.03366
.69134	.04416	−.03421	.05658	−.02911	.05542	−.02796	.05295	−.02548
.73570	.03868	−.02822	.05194	−.02025	.05097	−.01928	.04889	−.01720
.77779	.03304	−.02260	.04671	−.01192	.04592	−.01113	.04423	−.00944
.81720	.02739	−.01747	.04102	−.00468	.04040	−.00407	.03909	−.00275
.85355	.02193	−.01295	.03507	.00104	.03461	.00150	.03363	.00248
.88651	.01683	−.00911	.02903	.00495	.02871	.00527	.02801	.00597
.91574	.01223	−.00602	.02305	.00688	.02284	.00710	.02237	.00756
.94096	.00828	−.00366	.01726	.00696	.01712	.00710	.01683	.00740
.96194	.00508	−.00198	.01184	.00564	.01176	.00573	.01158	.00591
.99039	.00109	−.00026	.00333	.00173	.00331	.00175	.00326	.00180
1.00000	.00000	.00000	.00000	.00000	.00000	.00000	.00000	.00000

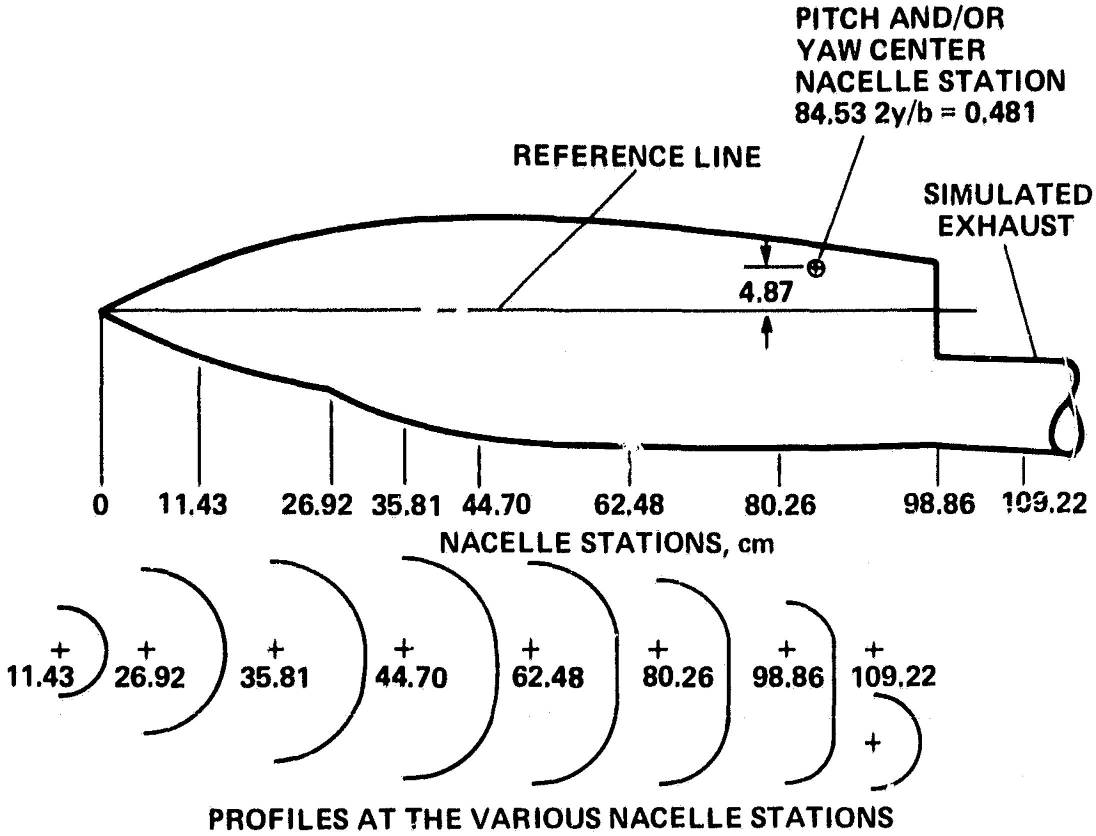

(a) Geometric characteristics.

Figure 1.– Nacelle geometry.

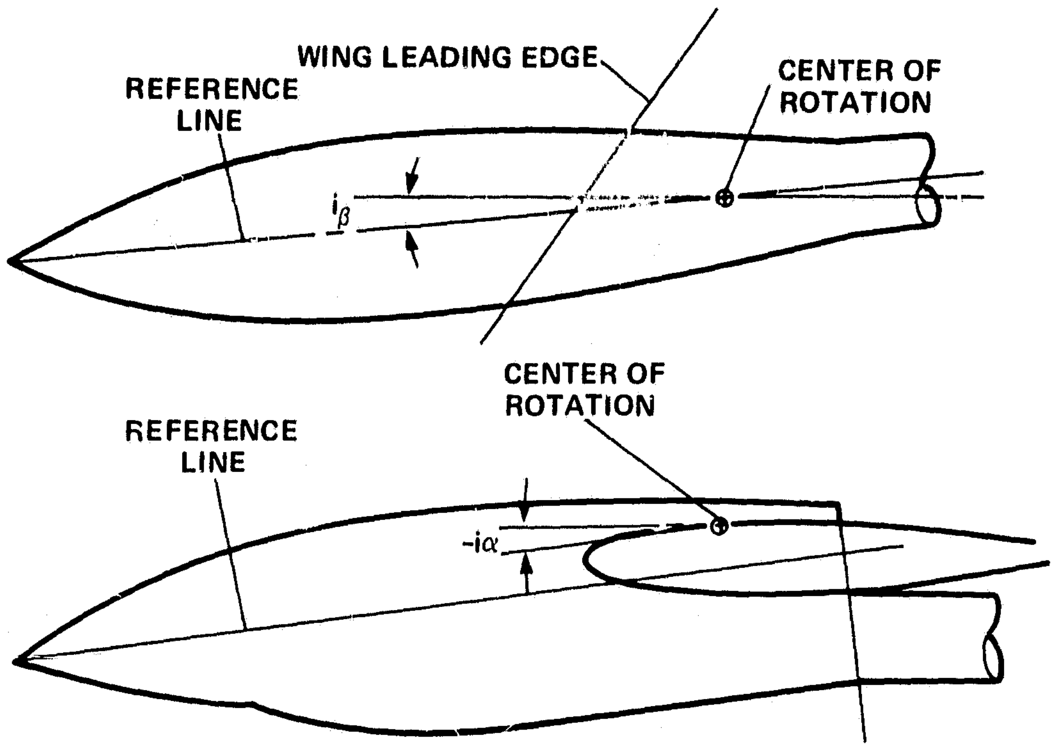

(b) Pitch and yaw sign convention.

Figure 1.— Concluded.

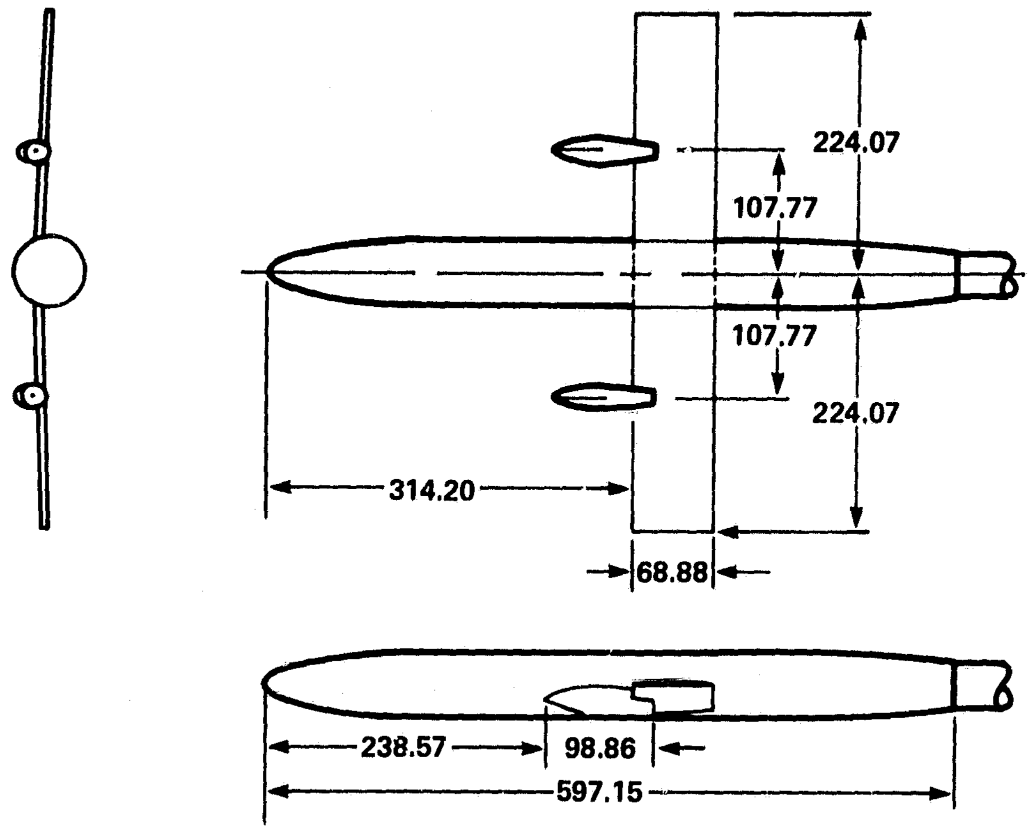

(a) PBW_1N configuration.

Figure 2.– Three-view drawing of model.

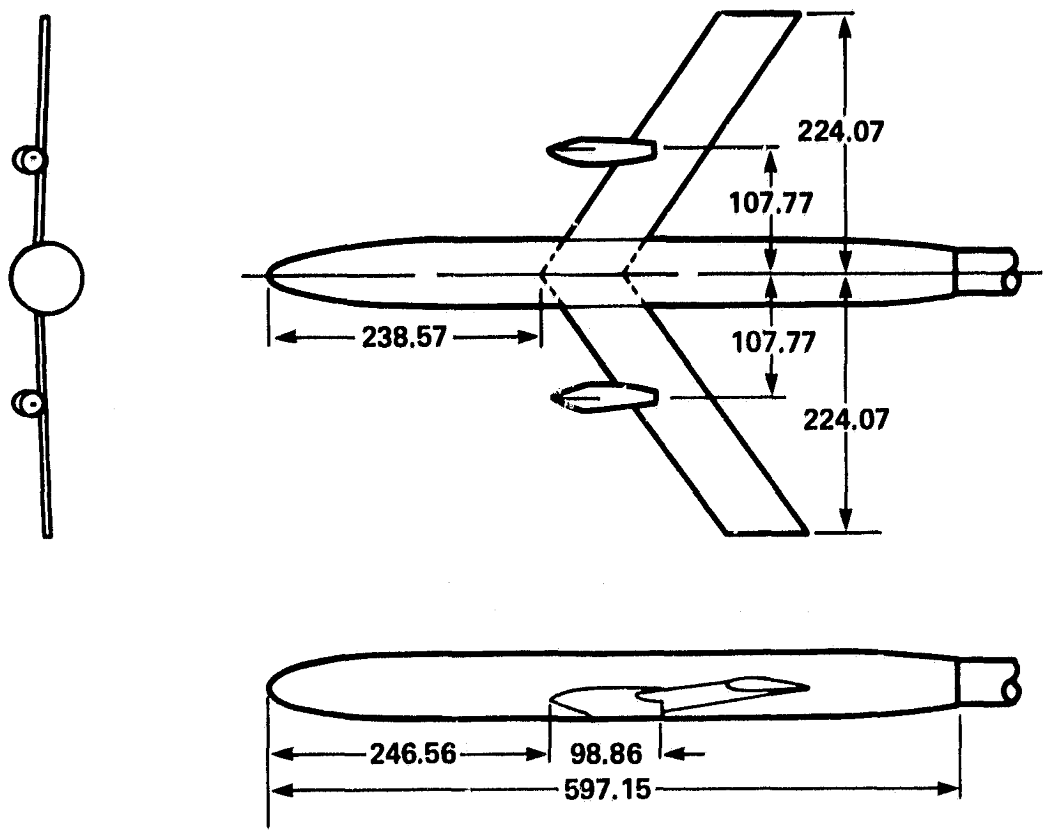

(b) PBW_2N configuration.

Figure 2.— Continued.

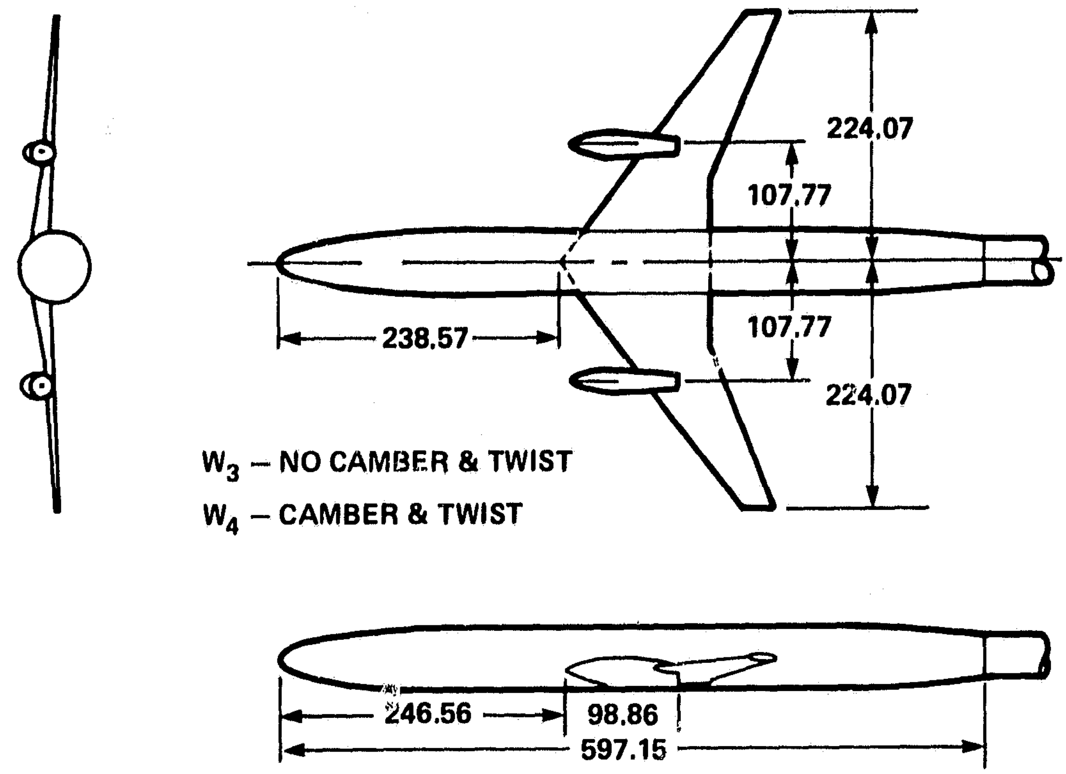

(c) PBW_3N and PBW_4N configuration.

Figure 2.– Concluded.

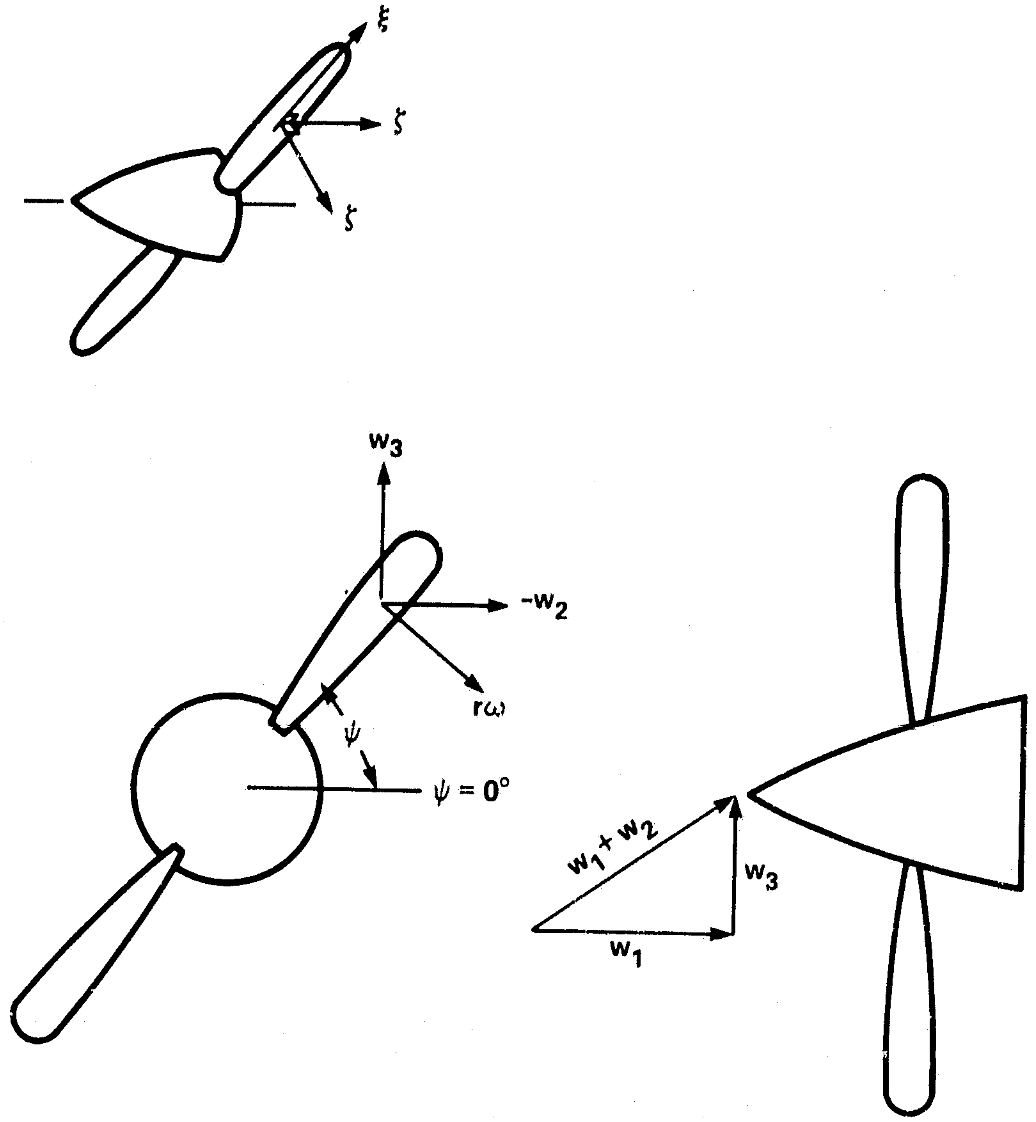

(a) Transformed velocities.

Figure 3.— Velocity diagram.

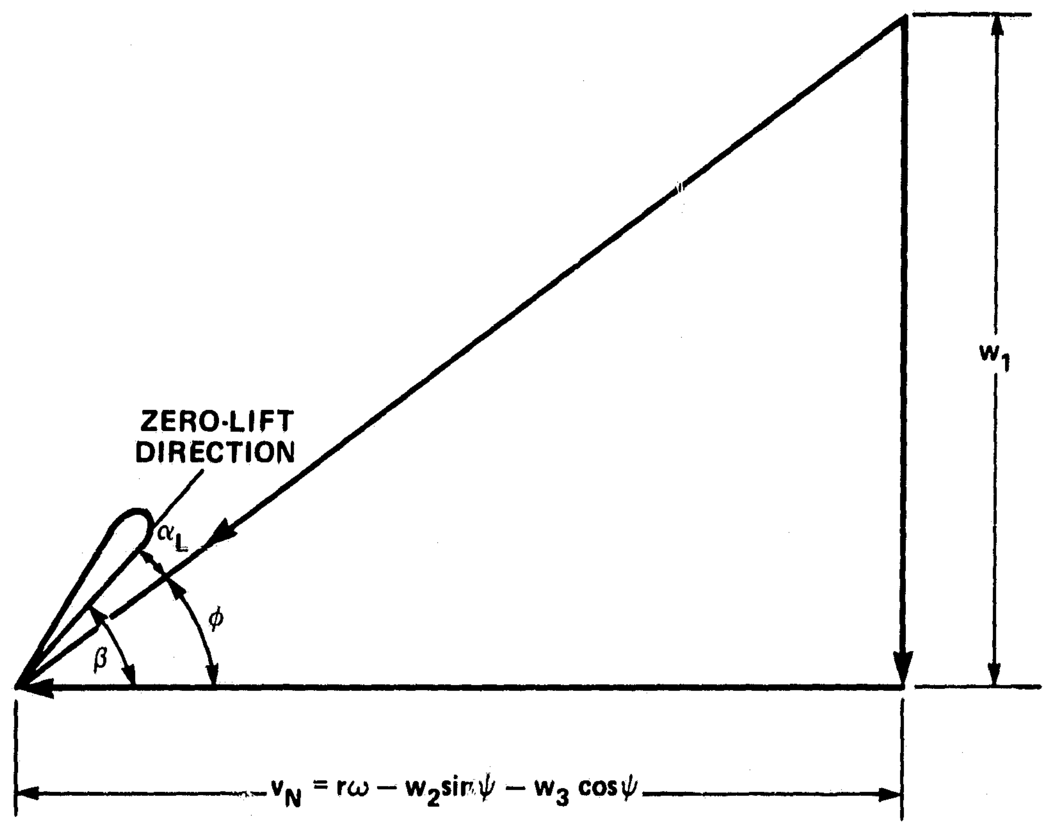

(b) Propeller section velocities.

Figure 3.— Concluded.

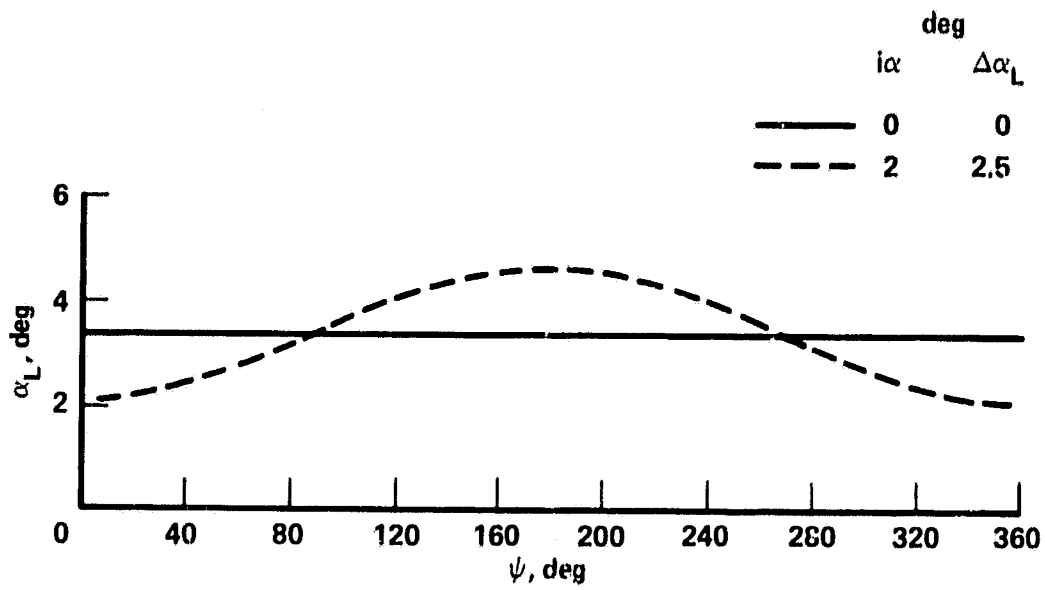

Figure 4.— Effect of propeller incidence on blade angle-of-attack characteristics for an isolated propeller; $i_\beta = 0°$.

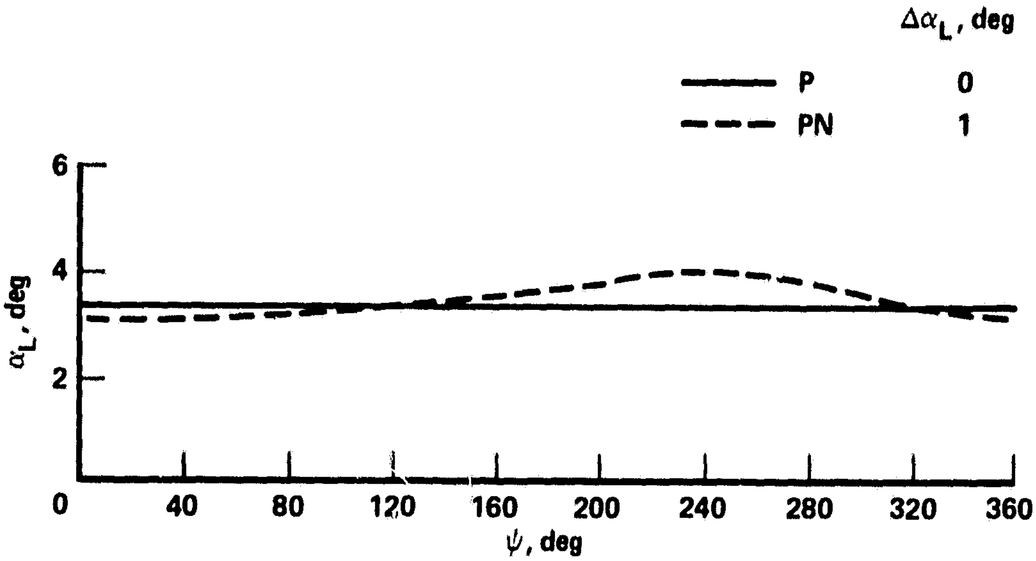

Figure 5.— Effect of the nacelle on the blade angle-of-attack characteristics of the propeller (P); $i_\alpha = 0°$, $i_\beta = 0°$.

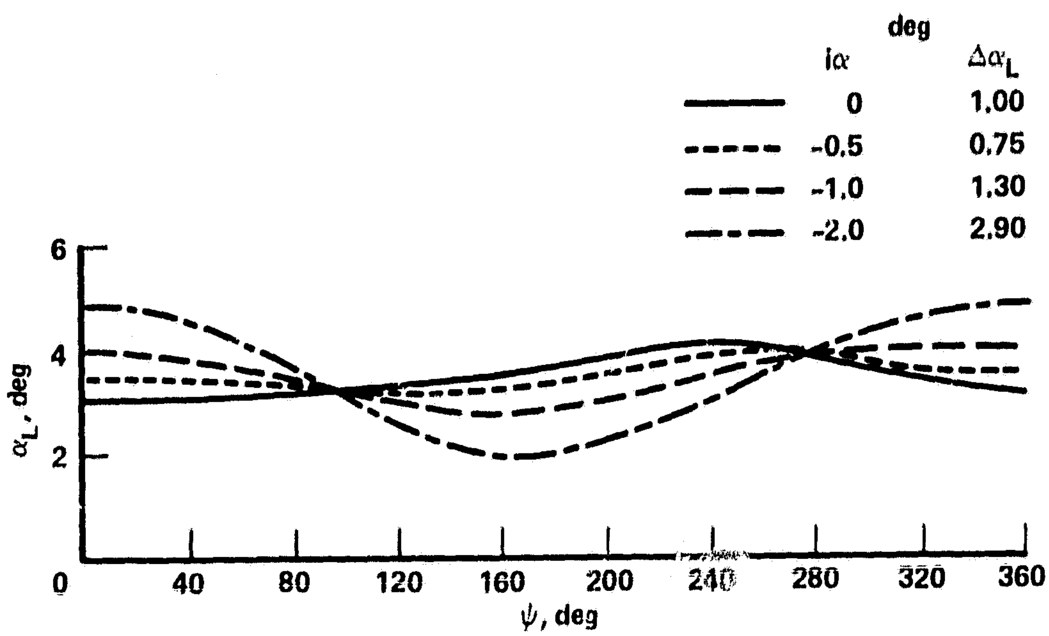

Figure 6.- Effect of nacelle incidence on the blade angle-of-attack characteristics of a propeller (PN); $i_\beta = 0°$.

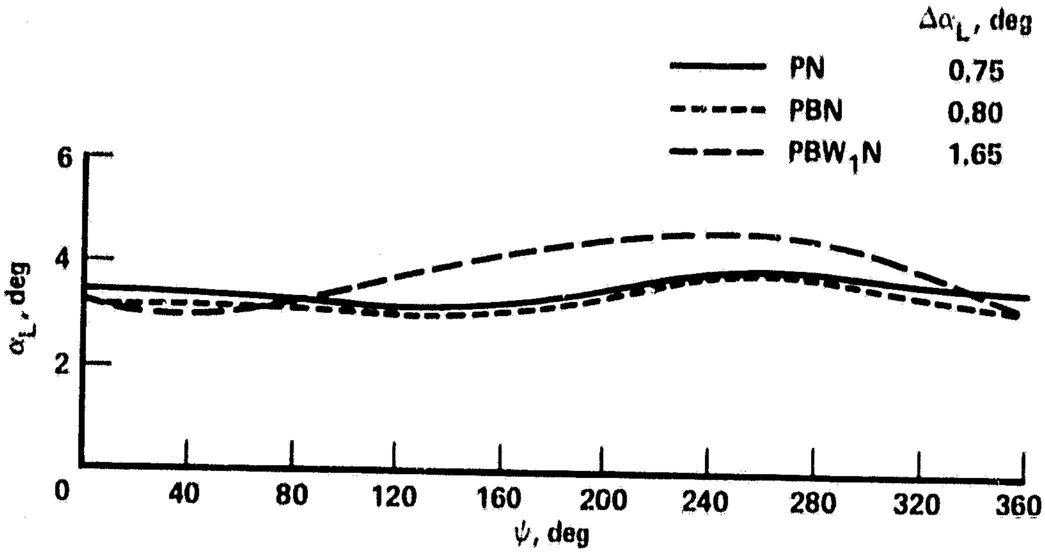

Figure 7.— Effect of configuration build-up on the propeller blade angle-of-attack characteristics; $i_\alpha = -2.5°$, $i_\beta = 0°$.

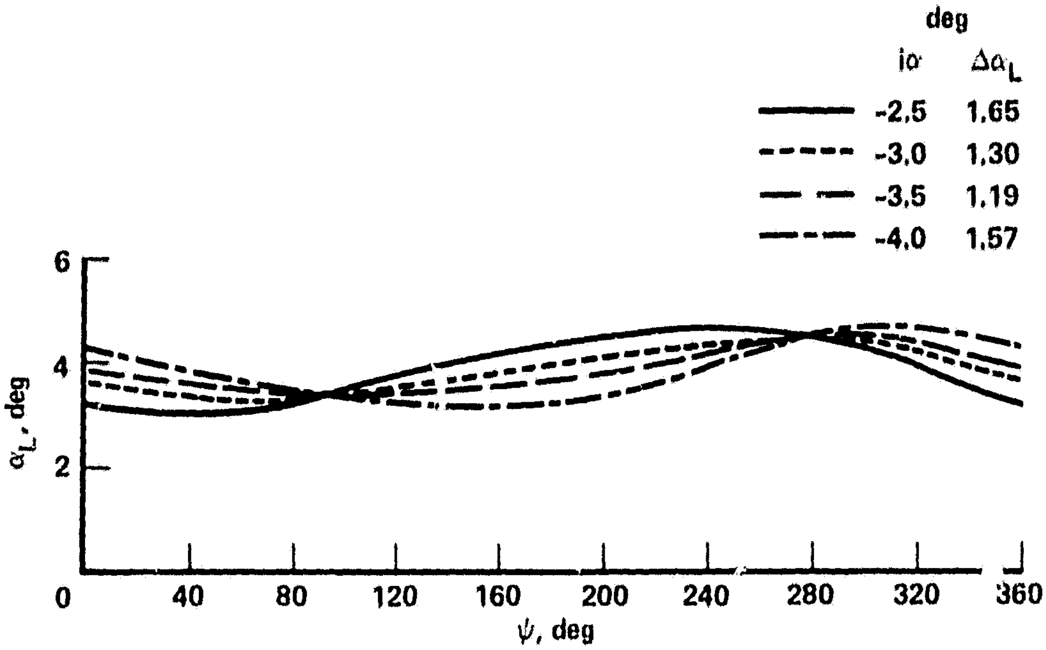

Figure 8.— Effect of nacelle incidence of the blade angle-of-attack characteristics for the PBW_1N configuration; $i_\beta = 0°$.

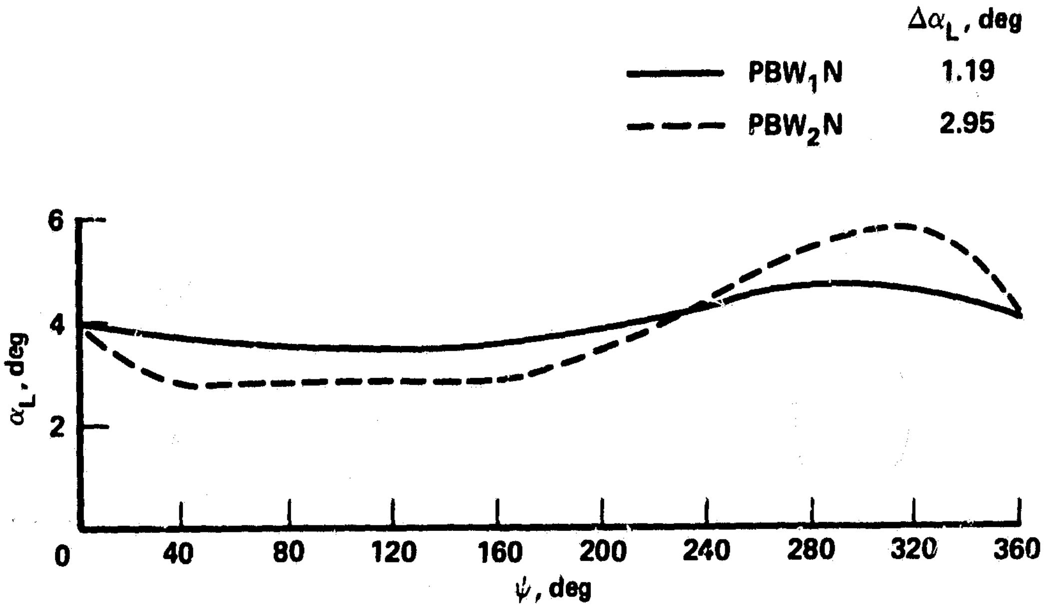

Figure 9.— Effect of wing sweep on the propeller blade angle-of-attack characteristics for the wing-body-nacelle configuration; $\alpha = 2°$, $i_\alpha = -3.5°$, $i_\beta = 0°$.

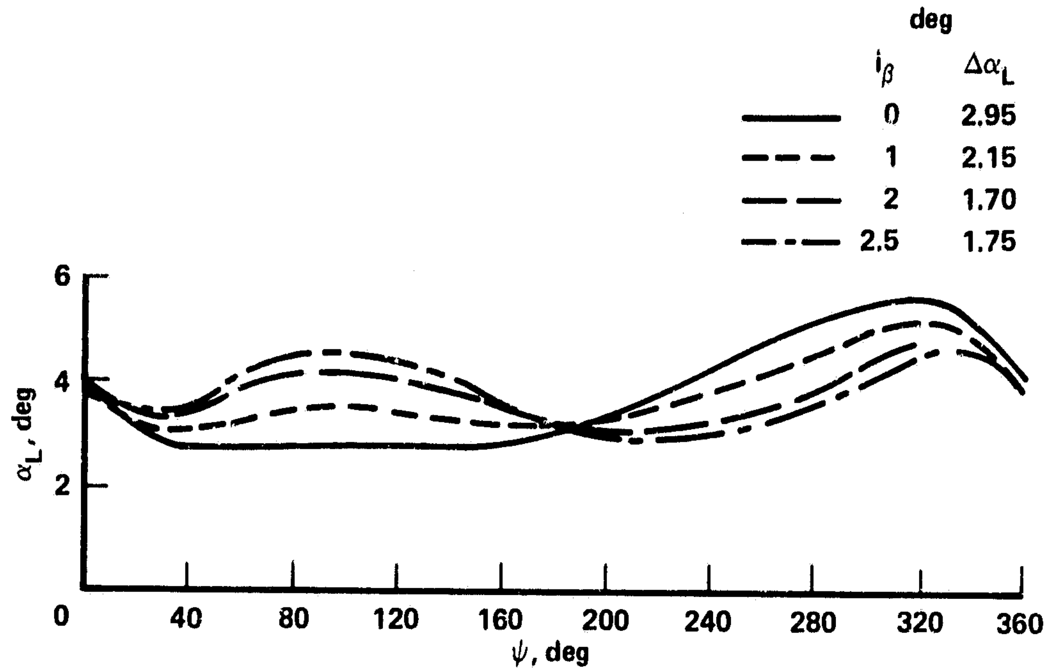

Figure 10.— Effect of nacelle yaw on the propeller blade angle-of-attack characteristics for the PBW_2N configuration; $\alpha = 2°$, $i_\alpha = -3.5°$.

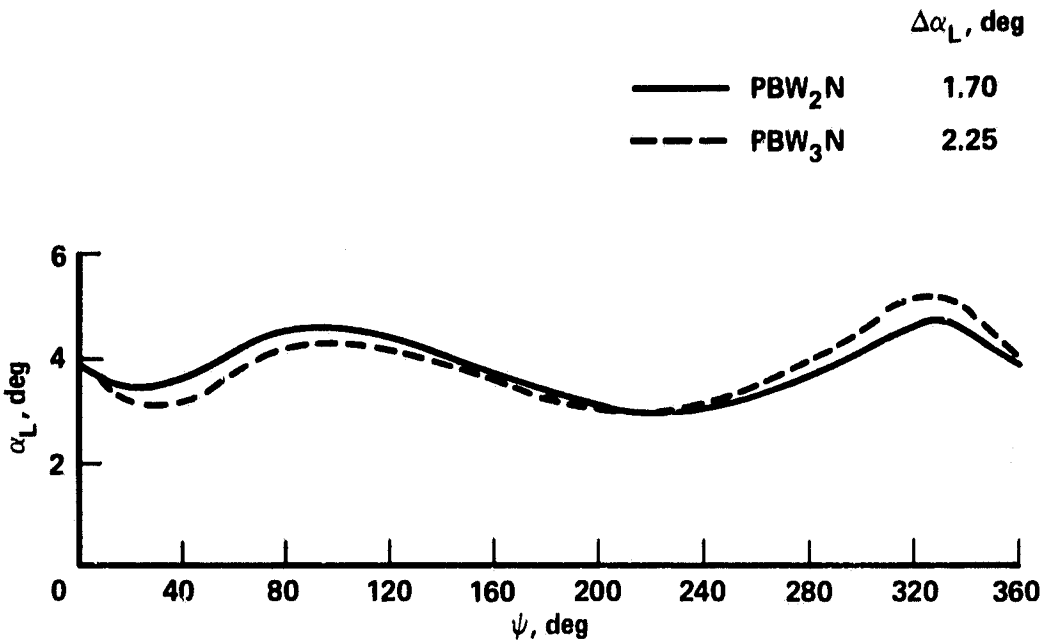

Figure 11.— Effect of wing planform taper on the blade angle-of-attack characteristics on the wing-body-nacelle configurations; α = 2°, i_α = -3.5°, i_β = 2°.

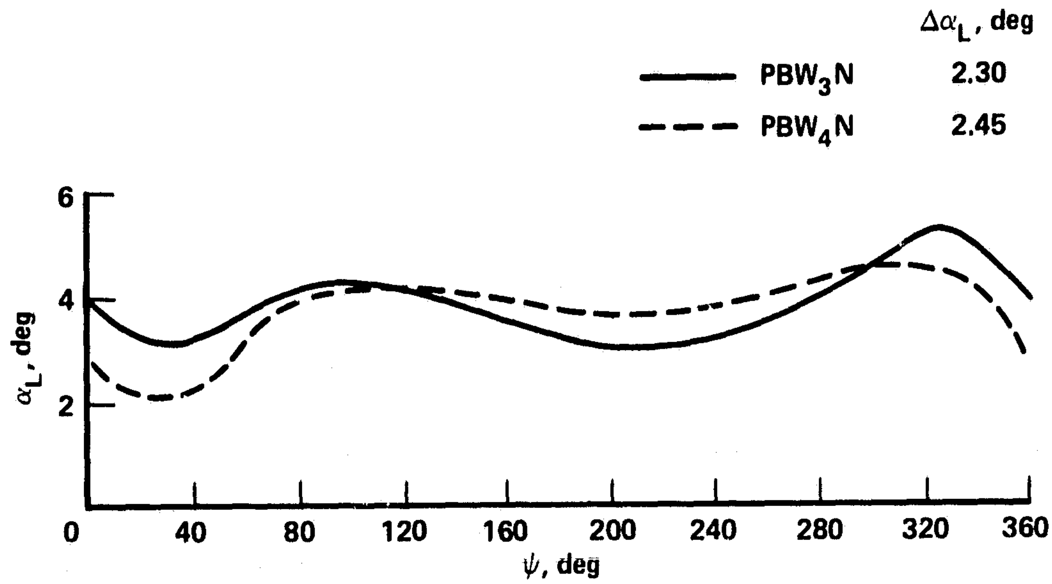

Figure 12.— Effect of wing camber and twist on the blade angle-of-attack characteristics for the wing-body-nacelle configuration; $\alpha = 2°$, $i_\alpha = -3.5°$, $i_\beta = 2.5°$.

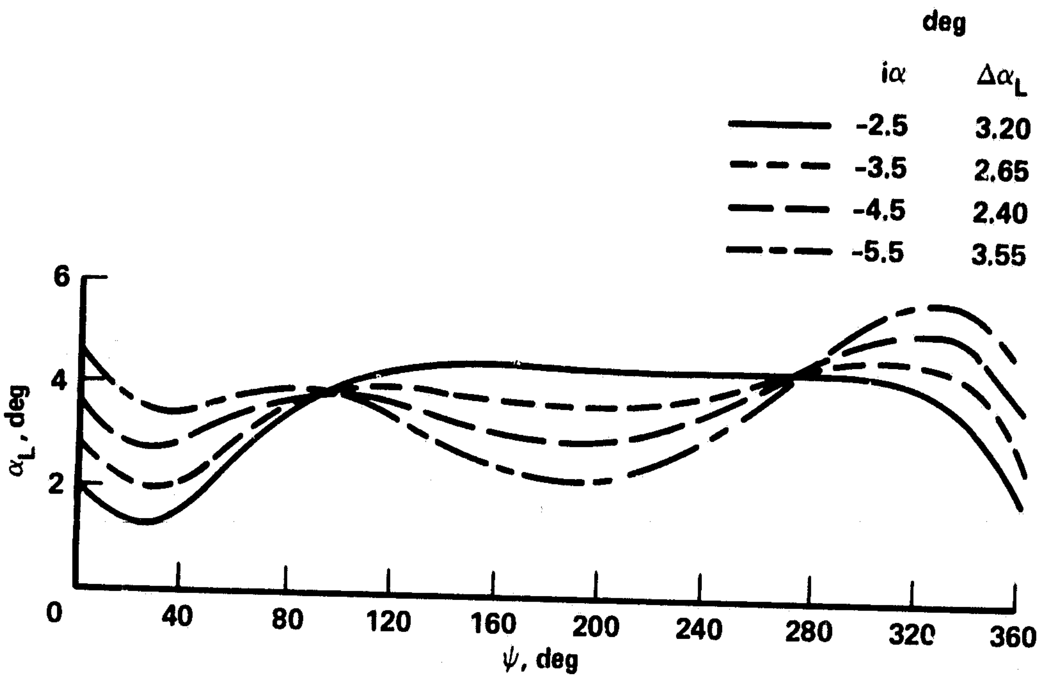

(a) $i_\beta = 2.0°$

Figure 13.— Effect of nacelle incidence on the blade angle-of-attack characteristics for the turboprop transport model (PBW_4N); $\alpha = 2°$.

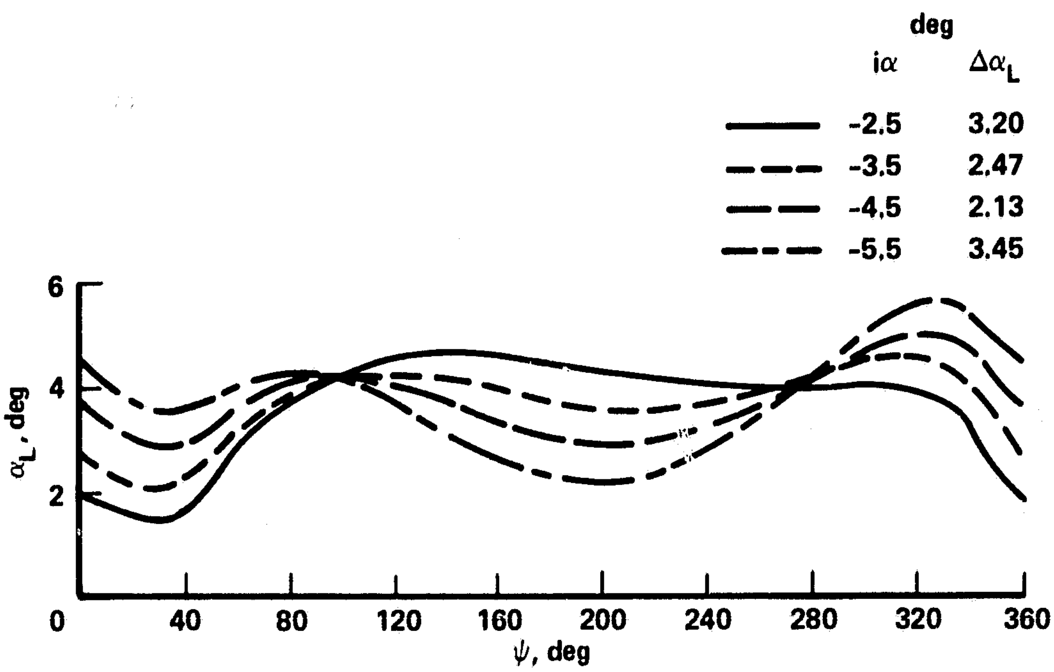

(b) $i_\beta = 2.5°$

Figure 13.— Continued.

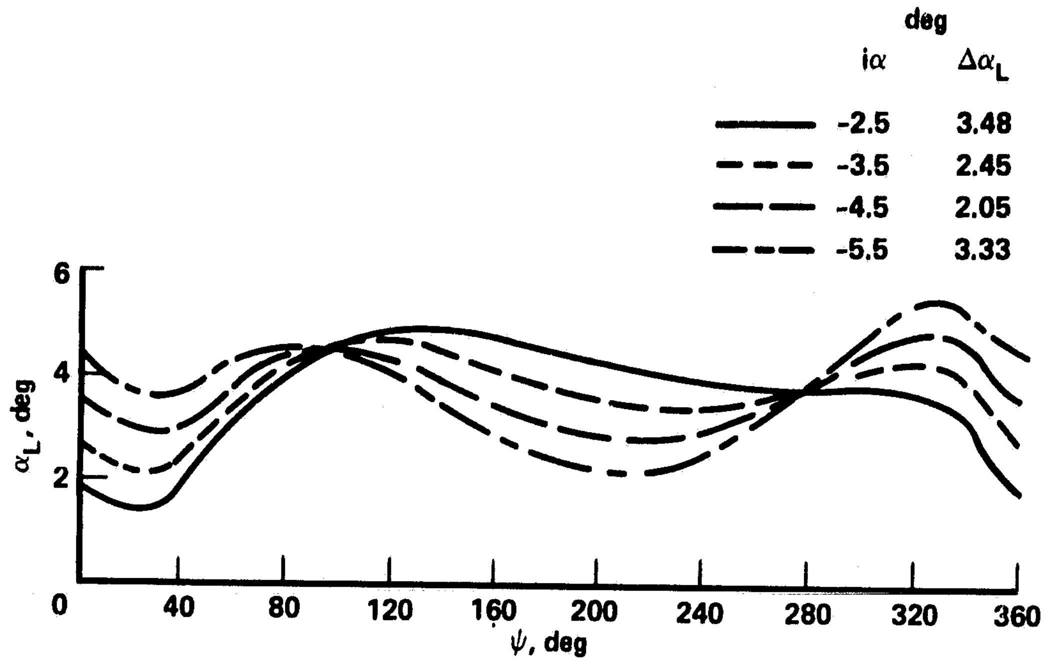

(c) $i_\beta = 3.0°$

Figure 13.— Continued.

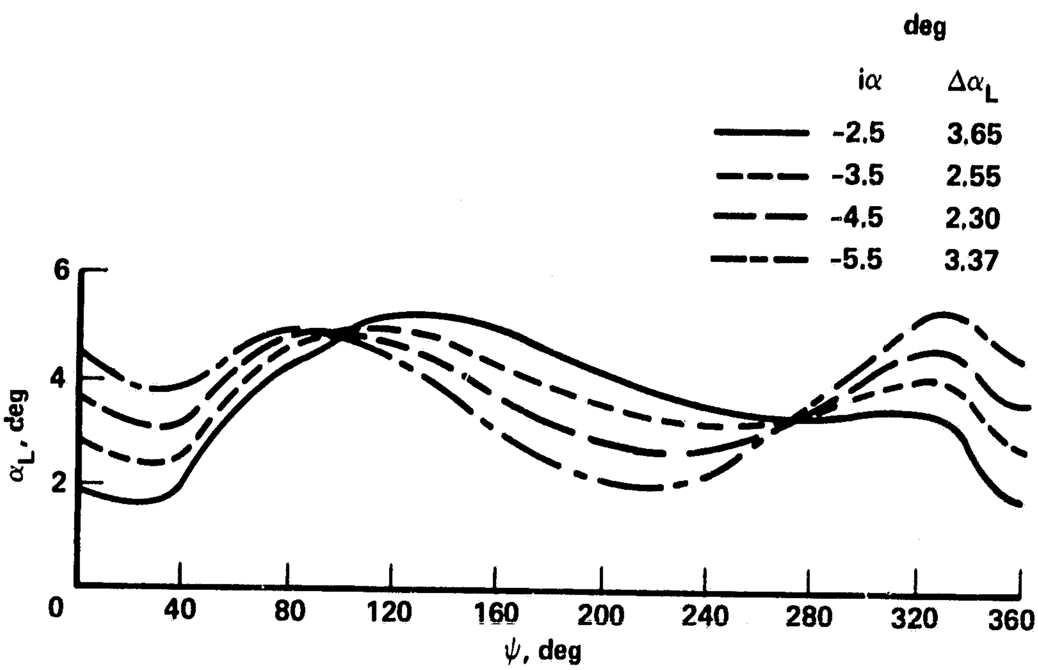

(d) $i_\beta = 3.5°$

Figure 13.— Concluded.

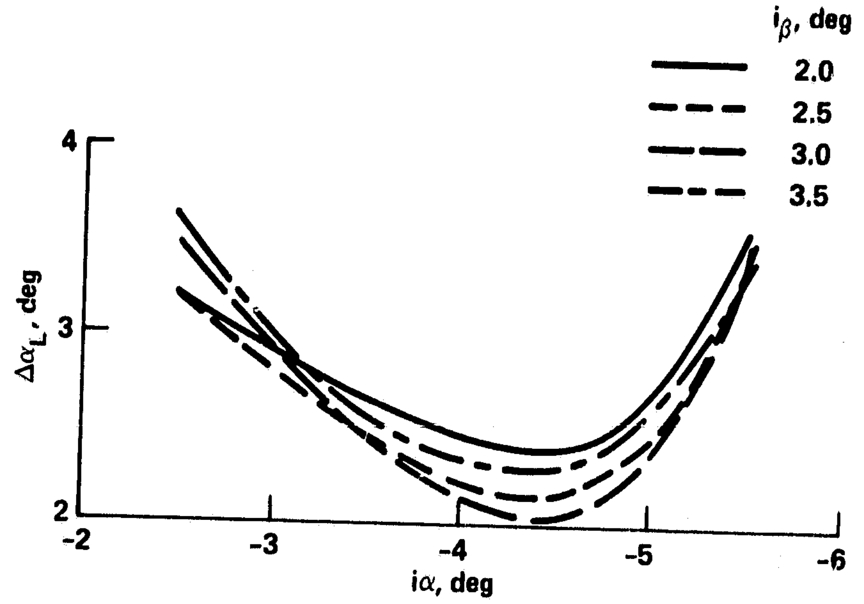

Figure 14.— Summary curves for the PBW_4N configuration.

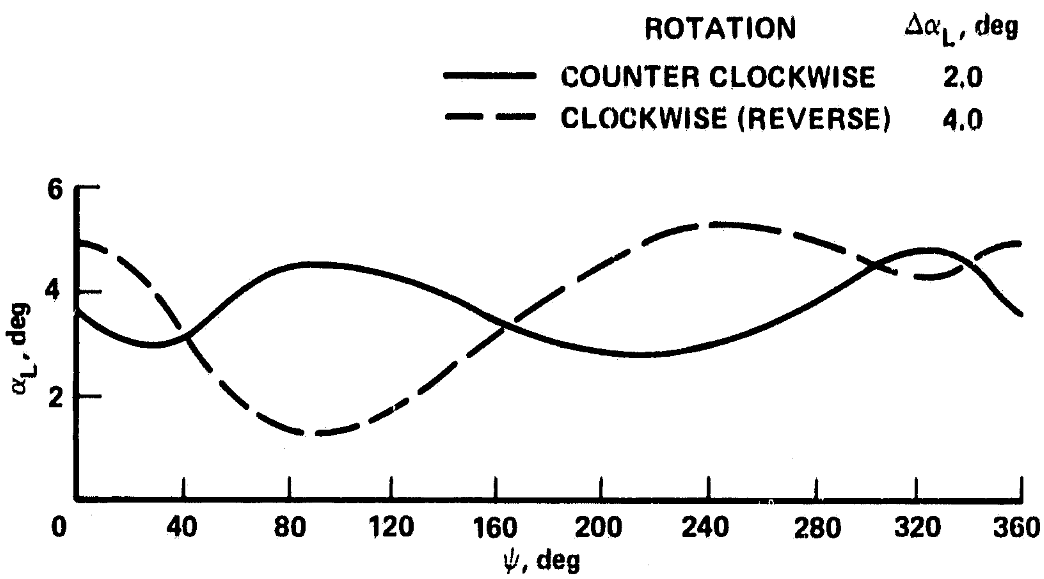

Figure 15.— Effect of reverse rotation on the propeller blade angle-of-attack characteristics for the turboprop transport model (PBW_4N); $\alpha = 2°$, $i_\alpha = -4.5°$, $i_\beta = 3.0°$.

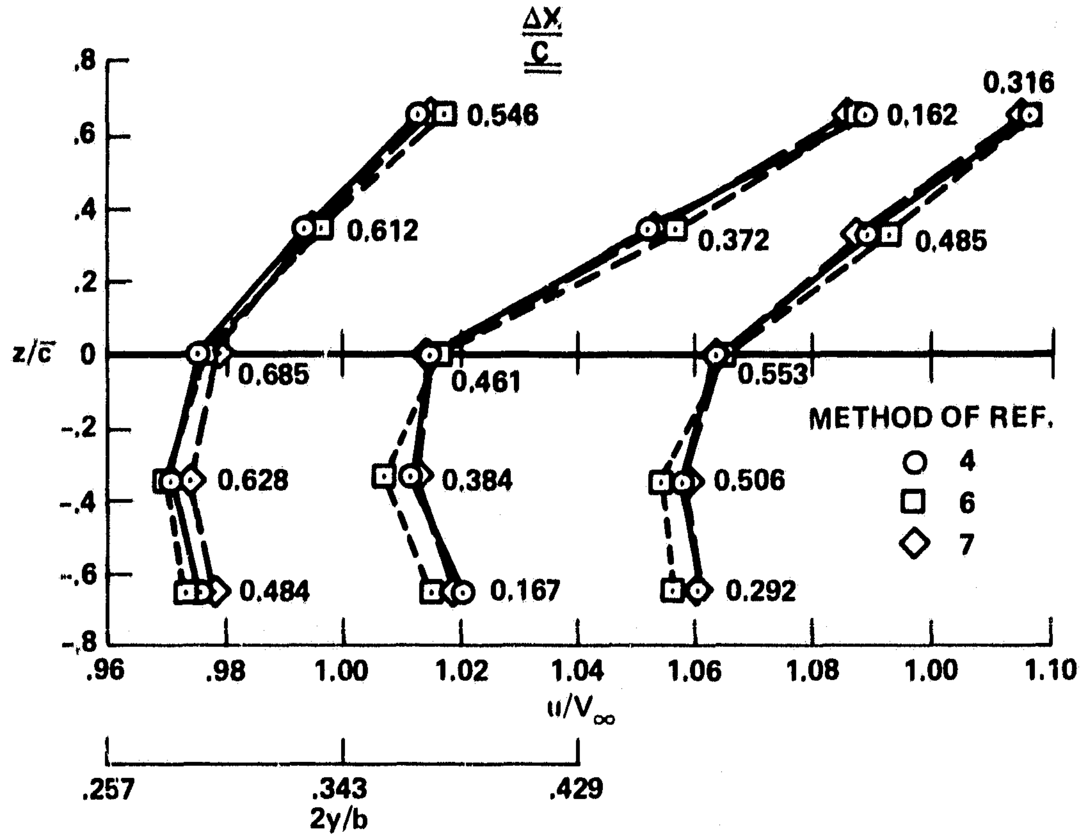

(a) x-component of velocity.

Figure 16.— Velocity components at off-body points for a wing alone computed by three different methods; M = 0.6, α = 2°.

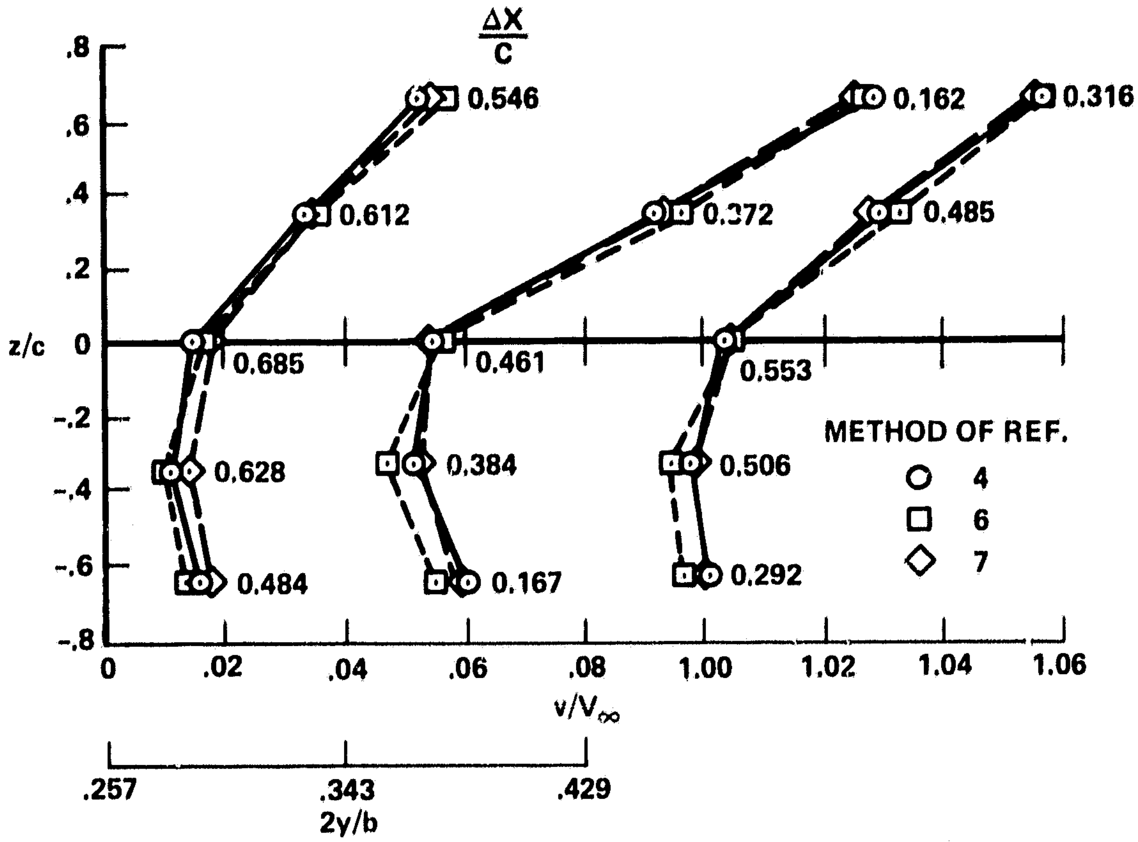

(b) y-component of velocity.

Figure 16.— Continued.

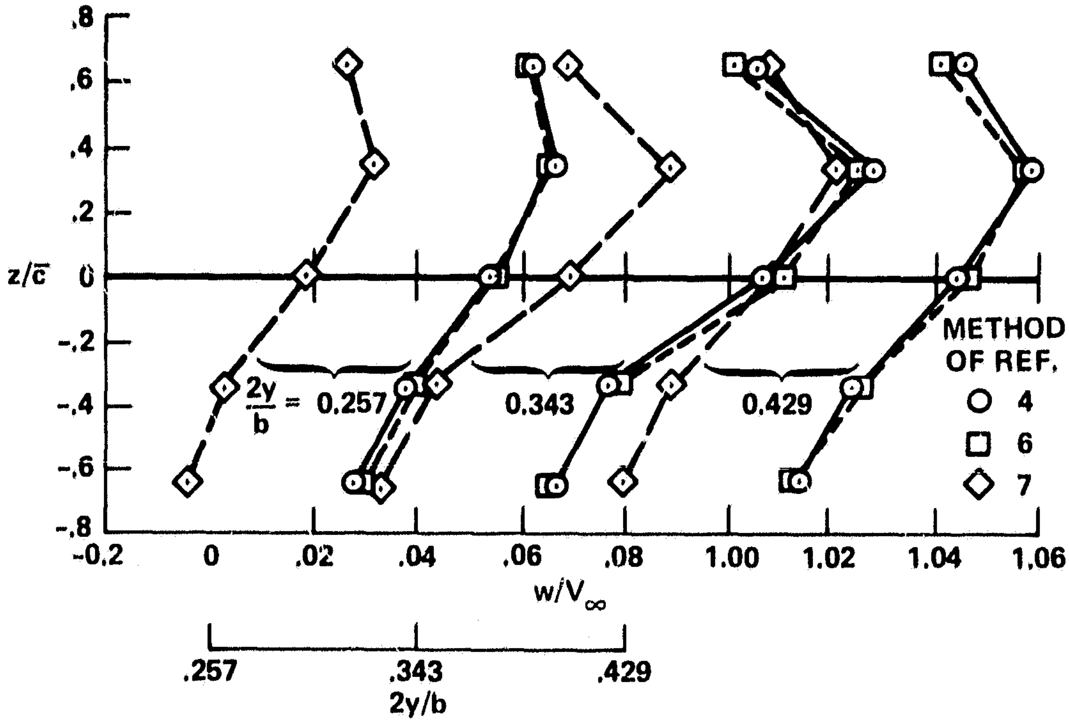

(c) z-component of velocity.

Figure 16.— Concluded.

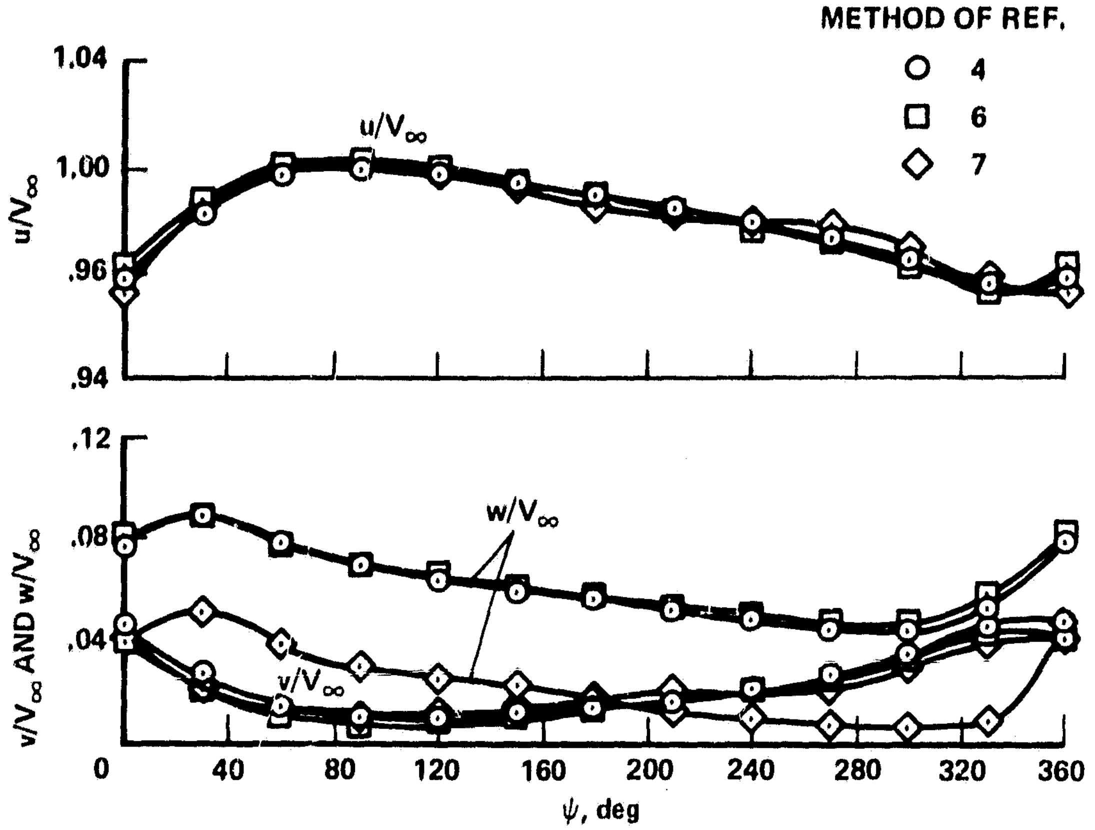

Figure 17.– Velocities in the plane of the propeller disc for a wing alone computed by three different methods; $\alpha = 2°$, $i_{\alpha} = -3.75°$, $i_{\beta} = 2°$.

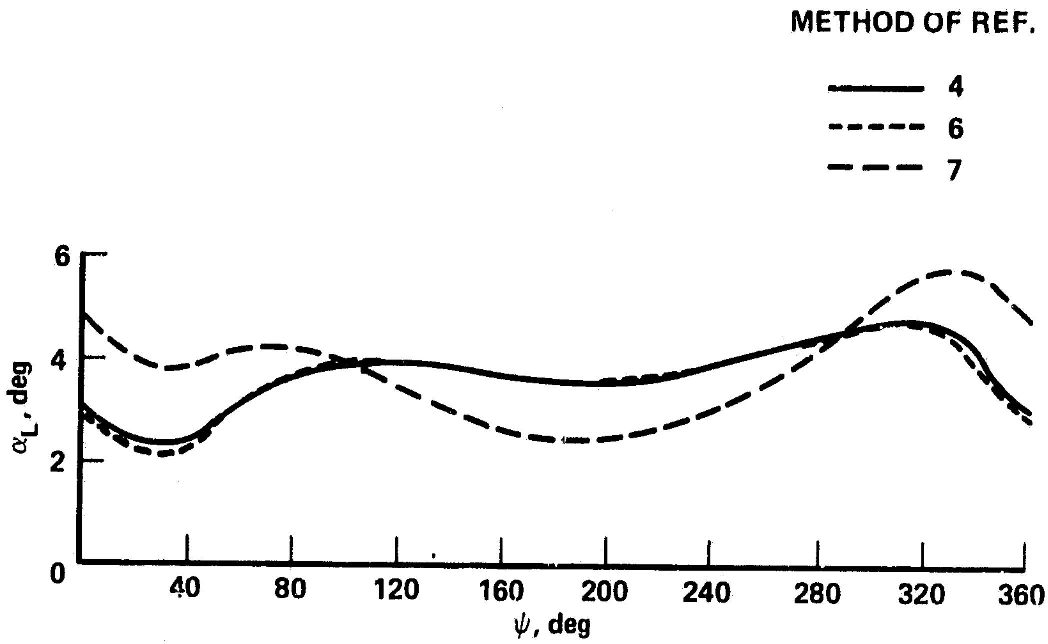

Figure 18.— Blade angle-of-attack characteristics computed by three different methods.

1. Report No. NASA TM-78587	2. Government Accession No.	3. Recipient's Catalog No.
4. Title and Subtitle INTERFERENCE EFFECTS OF AIRCRAFT COMPONENTS ON THE LOCAL BLADE ANGLE OF ATTACK OF A WING-MOUNTED PROPELLER		5. Report Date
		6. Performing Organization Code
7. Author(s) J. P. Mendoza		8. Performing Organization Report No. A-7812
		10. Work Unit No. 511-57-01
9. Performing Organization Name and Address Ames Research Center, NASA Moffett Field, Calif. 94035		11. Contract or Grant No.
		13. Type of Report and Period Covered Technical Memorandum
12. Sponsoring Agency Name and Address National Aeronautics and Space Administration Washington, D. C. 20546		14. Sponsoring Agency Code
15. Supplementary Notes		

16. Abstract

A brief theoretical study was conducted at $M = 0.6$ to obtain an understanding of the aerodynamic interference effects on a propeller operating in the presence of different wing-body-nacelle combinations. The study was directed toward minimizing the unsteady blade angle-of-attack variation with azimuth angle by varying the pitch and yaw of the nacelle. For the particular configuration of interest the minimum blade angle-of-attack variation occurred with the nacelle pitched downward 4.5° and yawed inward 3.0°.

17. Key Words (Suggested by Author(s)) Aircraft propulsion, Turboprop, Interference effects, Blade stress		18. Distribution Statement Unlimited STAR Category - 07	
19. Security Classif. (of this report) Unclassified	20. Security Classif. (of this page) Unclassified	21. No. of Pages 43	22. Price* $4.00

*For sale by the National Technical Information Service, Springfield, Virginia 22161